ACS Macro Letters

Letter

pubs.acs.org/macroletters

Confinement-Induced Crystal Growth in One-Dimensional Isotactic Polystyrene Nanorod Arrays

Hui Wu,[†] Yan Cao,[†] Ryohei Ishige,[‡] Yuji Higaki,[‡,§] Taiki Hoshino,[†] Noboru Ohta,[§] and Atsushi Takahara*[,†,‡,§]

[†]Japan Science and Technology Agency, ERATO, Takahara Soft Interfaces Project, Fukuoka 819-0395, Japan

[‡]Institute for Materials Chemistry and Engineering, Kyushu University, Fukuoka 819-0395, Japan

[§]Japan Synchrotron Radiation Research Institute/SPring-8, Hyogo 679-5198, Japan

[§]International Institute for Carbon-Neutral Energy Research (WPI-I2CNER), Kyushu University, 744 Motooka, Nishi-ku, Fukuoka 819-0395, Japan

Supporting Information

ABSTRACT: This work demonstrates the anomalous crystal growth of isotactic polystyrene (iPS) in nanorod arrays with different rod sizes. At the bottom of the nanorods, the crystals in bulk film grow into nanorods along either the [110] or [100] direction parallel to the rod axis. On the top side of the nanorods, the polymer exhibits different orientations corresponding to weak or strong confinement. In the weaker confinement (bigger nanorods of 300 nm diameter), the crystals grow with the [100] direction along the nanorod, which is similar to the crystals developed in the radial of spherulite. In the stronger confinement (smaller nanorods of 65 nm diameter), the splaying of crystals in the rod is significantly suppressed, and the preferred growth direction of iPS crystals is kept in either the [110] or [100] direction. The precise control of polymer crystal orientation and crystallinity at a local scale opens important perspectives for the design of one-dimensional nanomaterials whose performance depends on the anisotropic crystal properties.

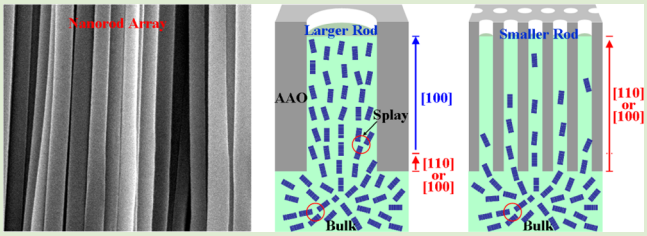

In nature, crystallization is one of the most common self-organization processes to form an ordered structure or pattern. Generally, complex crystalline entities like spherulites are produced by quenching liquids into crystalline solids in many materials, such as polymers, metal alloys, minerals, liquid crystals, and diverse biological molecules.[1] Without disturbance, a variety of semicrystalline polymers (polyethylene (PE), polypropylene (PP), poly(ethylene oxide) (PEO), isotactic polystyrene (iPS), etc.) usually crystallize as two-dimensional lamellar when being cooled from the disordered melt.[2−7] These crystals grow radially from a central nucleation site with a thickness of several tens of nanometers. The polymer chains oriented parallel to the lamellar surface normal and lateral dimensions of the lamellar were up to micrometers and eventually organized into (up to) millimeter scale three-dimensional spherulites with branched isotropic superstructures.

Recently, many efforts have been made to manipulate the structure and properties of semicrystalline polymers in nanoconfined dimensions. Crystallization determines the microscopic structure of the material, which affects the optical, electric, and mechanic properties. To control the properties of nanostructured materials in the development of nanotechnology, the ultrathin films,[1,8,9] droplets,[10] nanoimprint lithographies,[11] self-assembly of phase-separated block copolymers,[12−16] and infiltration of porous templates[17−29] are commonly used to build structures of nanosheets, nanocylinders, nanotrenches, and nanospheres. Because the primary nucleation, crystal morphology, growth rates, orientation, and crystallinity were affected by these confinements, the polymer crystallization depends on the geometry and dimension of isolated nanodomains. Therefore, the polymers in the confined dimensions exhibited unusual behaviors different from the bulk materials. For instance, the formation of spherulite superstructures is strongly suppressed in the polymer thin film, and a variety of unanticipated polycrystalline morphologies (e.g., dendrite, fractal crystals) are yielded.[1,8] As for the polymer in nanospheres,[13] crystallization is initiated by homogeneous nucleation, and the kinetics of the isothermal crystallization process follows first-order, which is different from the normal sigmoidal kinetics in the bulk.

Although the nanoconfinement effects on the morphology of the polymers have been the subject of many researches,[17−29] the effect on the crystal orientation in the one-dimensional nanodomain has not been extensively studied. The reported results showed that the polymer crystals in the nanocylinders

Received: March 17, 2013
Accepted: April 24, 2013
Published: April 29, 2013

exhibited a preferred orientation when the nanocylinders were examined as a whole entity. Nevertheless, the arising issues are, along the long axis of the cylinder, how the crystals grow and what the uniformity of crystal orientation is. To understand these issues, a detailed microstructural analysis for the crystal texture in the small sections of nanocylinders is desirable.

Therefore, we designed iPS nanorod arrays with two different rod sizes and represented the anomalous crystal orientation along nanorods with highly spatial resolution investigated using X-ray microdiffraction (micro-XRD).

The iPS nanorod array with rod diameters of 300 and 65 nm was prepared by melt-wetting the AAO templates with polymer melts via capillary force. Figure 1a shows optical micrographs of the 300 nm nanorod arrays released from the AAO templates. The dark area on the top is the nanorod array which is supported by the translucent bulk film on the bottom.[18] To analyze the iPS crystals developed in small sections of nanorod arrays from the bottom to the top, the thin slice of iPS nanorods/film was scanned from the top of the nanorods to the bulk with a step of 5 μm (Figure 1b). The total length of 300 and 65 nm diameter nanorods is about 118 and 111 μm, respectively. The interfacial boundary between the bulk and bottom of the rod was defined as an original position 0 μm. Thus, the positive positions 5−100 μm in Figure 1a correspond to the positions in the nanorod arrays from the bottom to the top, and negative position −25 μm is that of the reference bulk film, respectively.

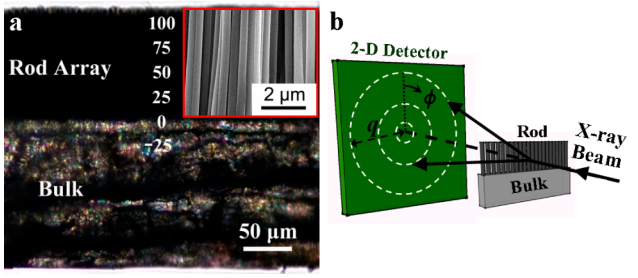

Figure 1. Typical optical micrographs of a thin slice of iPS nanorod arrays/bulk of 300 nm during the micro-XRD measurement. Inset of (a) is the SEM images of iPS nanorod arrays. (b) Schematic illustration of the X-ray microdiffraction geometry employed for investigating the iPS crystals developed in the nanorod arrays. The interface between the bulk and rod array was defined as position 0 μm, and the thin slice was scanned with a step of 5 μm.

Figure 2 shows the representative two-dimensional (2D) micro-XRD patterns of nanorod arrays/bulk of 300 and 65 nm at selected positions in the thin slice. Referring to the hexagonal cell (a = b = 2.19 nm and c = 0.665 nm) of iPS crystals proposed by Natta and Corradini,[30] the reflections located at the q values of 5.6, 9.8, 11.4, 13.0, and 15.5 nm^{-1} are indexed as (110), (300), (220), (211), and (410)/(311), respectively, as shown in the pattern of bulk film at position −25 μm (Figure 2a,b).

To understand the 1D diffraction profiles extracted from the azimuthal integration of the 2D diffraction patterns, the total intensity of the diffraction at different positions in 300 and 65 nm nanorods plotted against the scattering vector (q) is shown in Figure 3a and 3b, and the degree of crystallinity of iPS at different positions is shown in Figure 3c. The relative crystallinity was evaluated from the equation[31] $X_c = \Sigma I_c/\Sigma(I_a + I_c)$, where I_c is the integrated area underneath the crystalline peaks and I_a is the integrated area of the amorphous halo, estimated by the peak-fitting of the 1D intensity profiles. The crystallinity of nanorods with 300 nm diameter is about 36.1 ± 1.9%, and the crystallinity of bulk film is about 35.3 ± 2.0%. The relative standard error of crystallinity of 300 nm nanorods is about 5.3%, which shows no measurable difference along the rod and that the crystallinity at different rod positions as shown in Figure 1a is almost identical. In the nanorods of 65 nm diameter, the crystallinity decreased from the bottom to the top, lower than the bulk, and almost vanishes at the top of the nanorods. The gradient distribution of crystallinity in nanorods obtained by the XRD measurements is in accordance with the reported FTIR observations.[23]

In the 2D diffraction patterns, the intensity of (220) and (300) reflections depends on the azimuthal angle ϕ (ϕ = 0° corresponds to the meridian) for these two different confinements at various positions, showing an anomalous polymer crystal growth. Figure 3d, e, g, h shows the integrated intensities of (220) and (300) diffraction against ϕ in nanorods of 300 and 65 nm diameters, respectively. In the larger nanorods of 300 nm diameter, two distinguished crystal orientations on the bottom and top were observed. At position 5−15 μm, the maximum diffraction intensity of both (220) and (300) is centered at ϕ = 0°, indicating that the crystals either with [110] or with [100] growth directions are preferred aligned along the rod direction. At the upper positions 20−110 μm, the maximum diffraction intensity of the (220) shift to ±30° and six symmetric appearances at ±30°, ±90°, and ±150° can be observed. The maximum diffraction intensity of (300) is

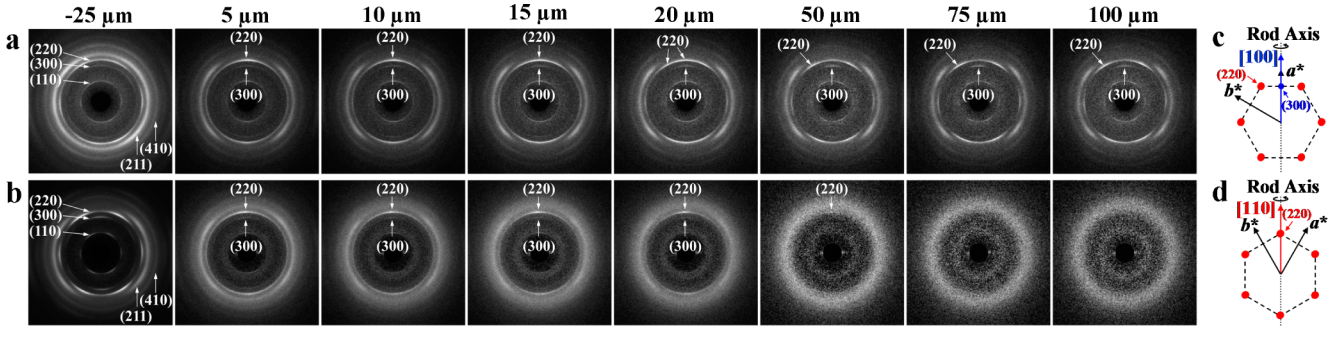

Figure 2. Typical 2D micro-XRD patterns of nanorod arrays/bulk of 300 nm (a) and 65 nm (b) at positions of bulk film reference: −25 μm and nanorod arrays: 5, 10, 15, 20, 50, 75, 100 μm. Reciprocal space construction of the diffraction pattern of the (c) [100] direction and (d) [110] direction along the rod direction when a hexagonal unit cell is assumed.

dx.doi.org/10.1021/mz400136d | ACS Macro Lett. 2013, 2, 414−418

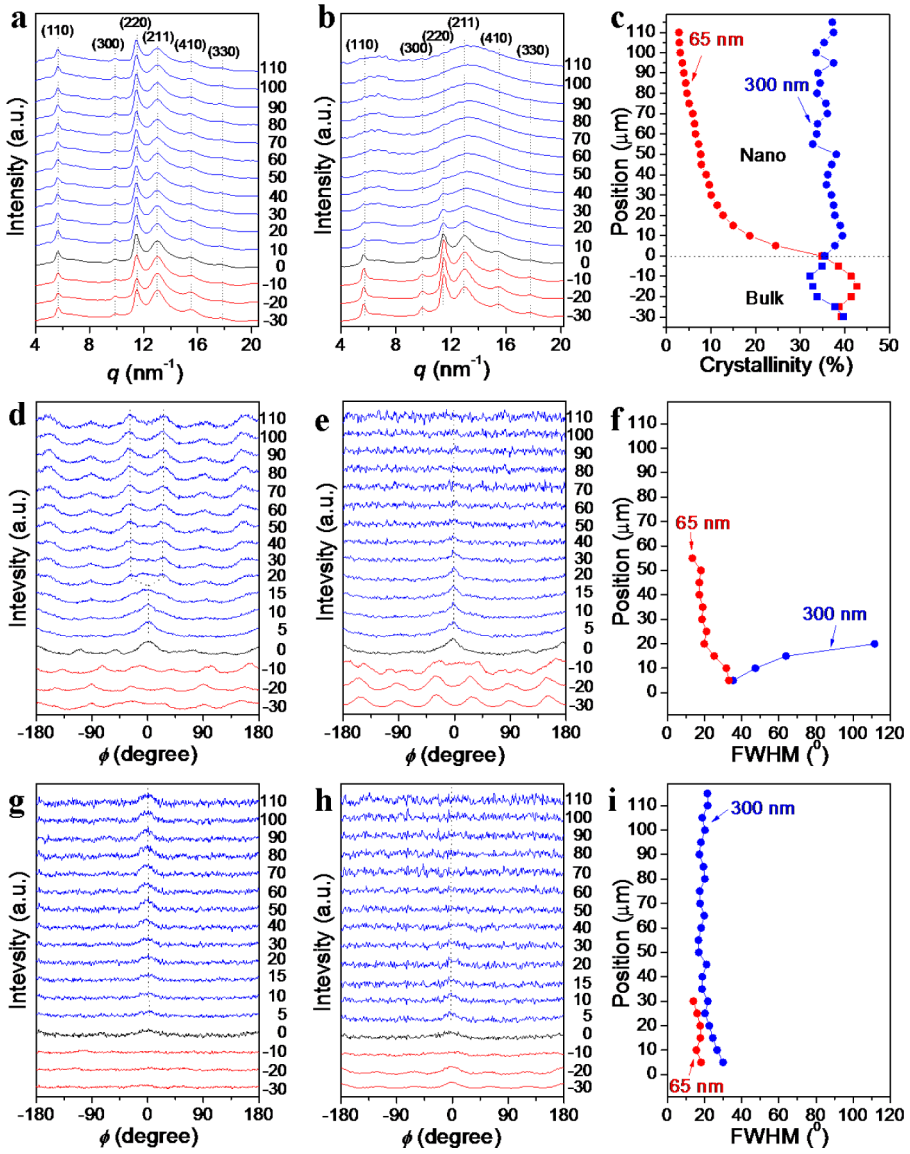

Figure 3. 1D intensity profiles of nanorods/bulk film in nanorods of (a) 300 nm and (b) 65 nm calculated by the azimuthal integration of the 2D-diffraction patterns. (c) The degree of crystallinity of 300 and 65 nm nanorods at different positions. Azimuthal intensity distribution of the (220) reflection in nanorod arrays of (d) 300 nm rod and (e) 65 nm rod and that of the (300) reflection in nanorod arrays of (g) 300 nm rod and (h) 65 nm rod. Full width at half-maximum (fwhm) of (220) reflection (f) and (300) reflection (i) in nanorods at different positions.

along the rod direction. These patterns correspond to the orientation that the [100] direction is parallel to the rod long axis (Figure 2c).[32] For the 65 nm rods at different positions, the maximum diffraction intensity of both (220) and (300) diffractions only appears at $\phi = 0°$ along the nanorods. This implies that a uniform crystal orientation goes through the whole nanorod. The [110] direction of crystallites was the preferred crystal growth direction as well as the [300] direction.

To evaluate the crystal orientation, the full width at half-maximums (fwhm) of (220) and (300) X-ray reflections in nanorods were analyzed. Because of the low crystallinity in the upper side of 65 nm nanorods, we simply analyze the (220) and (300) reflections with distinguishable intensity located at the meridian. As shown in Figure 3f, for the (220) diffraction in the nanorod array of 300 nm diameter, the value of $\text{fwhm}_{(220)}$ tends to increase from position 5 μm to position 20 μm, indicating that the larger nanopores had less confinement on (220) diffraction and the crystallite orientation was changed from the [110] direction to the [100] direction. In the 65 nm rod, $\text{fwhm}_{(220)}$ has a trend to decrease from position 5 μm to position 60 μm, implying that the smaller pore has a profound confinement effect on this crystallite orientation. As for the (300) reflection in Figure 3i, the $\text{fwhm}_{(300)}$ of the 300 nm nanorod array decrease from position 5 μm to position 20 μm and maintains a stable value at positions of 25−115 μm. In the nanorods of 65 nm, the $\text{fwhm}_{(300)}$ value is slightly lower than that in the corresponding positions of the 300 nm nanorod array. This distinctly shows that the degree of crystal orientation in smaller nanorods is considerably improved compared to that in the larger ones due to the stronger confinement.

To determine the fast growth direction in the crystals, the micro-XRD measurement on the iPS thin film were also performed. When iPS crystallizes from the melt in the bulk film, the crystallization is initiated by the defects and impurities existing in the polymers and forms isotropic spherulite with a

dx.doi.org/10.1021/mz400136d | ACS Macro Lett. 2013, 2, 414−418

bunch of branches to fill the whole volume completely.[6,32] In the 2D-diffraction patterns of spherulites (see Supporting Information), the spherulite was grown with the [100] direction as the radial direction. Therefore, we can speculate that to achieve the spherical shape at the temperature of 443 K the secondary nucleus develops at the growth front of radiating fibrils that splay into branches.[4,9] The splaying branches of the lamellae cause the crystals to grow with the [100] direction as a radial direction.

In the isothermal crystallization process of iPS bulk film observed by polarized optical microscopy (POM) at 443 K, the nucleation density is evaluated to be ~2.7×10^{-6} nuclei/μm^3 (see Supporting Information), which is less than the reported value of 0.4 nuclei/μm^3.[33] This is because the iPS samples used were filtered in a fractionation process, and then most of the impurities and particulates were removed. For a larger nanorod with a diameter of 300 nm and a length of 118 μm, a rod only contains 2.3×10^{-5} nuclei, while in a smaller nanorod of 65 nm diameter and 111 μm length the nuclei number is 1.0×10^{-6}. Although few nuclei randomly can form at the internal surface of the nanopores,[28,34] heterogeneous nucleation is not an efficient process for both of these isolated nanorods. Because of the extremely low nucleation density, the crystallization of iPS in the isolated nanorods is significantly suppressed,[22] and then lots of separated nanorods were still in the amorphous state and were not crystallized.

Because the nanorods were connected with a bulk reservoir, the bulk crystallization dominates the crystallization of nanorods.[17,23] The crystals (fibrils in the spherulites) formed in the bulk hit the amorphous nanorods and act as a secondary nuclei to initiate the crystallization at the bottom of the nanorods. Therefore, the crystals with either [100] direction (Figure 2c) or [110] direction (Figure 2d)[32] favor to grow into nanorods. Due to the gate effect,[17] the crystal growth selectively follows an unrestricted pathway to maintain its growth. Only the lamellae with the orientation coincident with the rod direction are able to grow into the pores. Therefore, either the [110] or [100] growth direction is in accordance with the long axis of the rod in the bottom of nanorods of 300 and 65 nm diameter (position from 5 to 15 μm), yielding that the *c*-axis of the crystals in the nanorods is preferentially perpendicular to the rod long axis.[17,23]

As the crystals grow to the position of 20 μm in larger nanorods of 300 nm diameter, due to weaker confinement, the crystals[4,9] splay apart and branch at the growth front of the fibrils to fill the volume of the nanorod. The crystals grow with the [100] direction. This cylindrical confinement-induced one-directional growth is similar to the crystals that developed along the radii of spherulite. Thus, the crystals in the upper position of the nanorod from 20 to 115 μm prefer to grow with the [100] direction along the nanorod long axis with identical crystallinity (Figure 4a).

In the upper position 20−115 μm of smaller nanorods of 65 nm diameter, the growth of fibrils is inhibited by the stronger confinement of cylindrical nanopores. The branching and splaying in the spherulite formation is suppressed, which was manifested by the decreased fwhm value as compared to that of larger nanorods. The crystals keep growing along the original direction. Thus, either the [100] or [110] direction was the preferred crystal growth direction in the smaller nanorods (Figure 4b). However, only the strictly aligned crystals with [*hk*0] direction along the rod direction can grow, and other growth (off-rod direction) will stop by the pore wall. This causes the iPS crystallites to decrease from bottom to top with gradient crystallites.

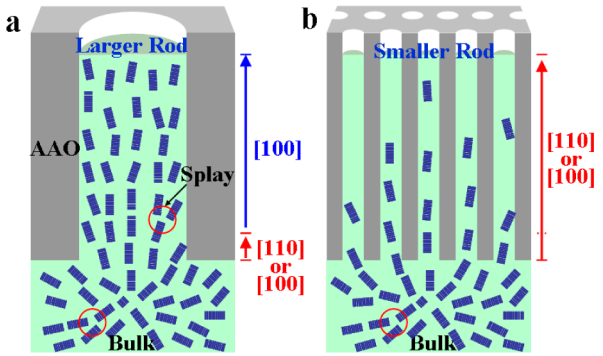

Figure 4. Schematic illustration of iPS crystals developed in (a) larger nanorods of 300 nm diameter and (b) smaller nanorods of 65 nm diameter.

In summary, the anomalous crystal growth in iPS nanorod arrays of different rod diameter was investigated by micro-XRD. Due to the lack of nuclei in nanorods, the polymer crystallization of the nanorods was initiated by the crystals formed in the bulk. At the bottom of the nanorods, the crystals grow into nanorods from bulk film with either [110] or [100] direction. In the upper of the nanorods, the polymer crystals developed in the different confinements exhibit different orientation and crystallinity. For the polymer in the weaker confinement (larger nanorods of 300 nm diameter), the crystals grow with preferred [100] direction along the rod with identical crystallinity, which is similar to the crystals developed in the radial of spherulite. When the polymer is in the stronger confinement (smaller nanorods of 65 nm diameter), the branching and splaying in the spherulite formation at the growth front is significantly suppressed. The crystallites were kept growing from bottom with either [110] direction or [100] direction along the rod with gradient crystallinity. The ability to control polymer crystal orientation and crystallinity at a local scale opens important perspectives for the design of the 1D nanomaterials whose performance depends on the anisotropic crystal properties.

EXPERIMENTAL SECTION

Materials. iPS was kindly supplied by Idemitsu Kosan Co., Ltd. After fractionation,[23] iPS with M_n of 121 000 (M_w/M_n = 1.16) and isotacticity of ~100% was obtained. The AAO templates with pore diameters of 300 and 65 nm and length of 140 μm were prepared by a two-step anodization process.[35,36] To prepare the polymer nanorods, the AAO templates with diameters of 300 and 65 nm were placed on top of a 200 μm thick amorphous iPS film. After annealing the AAO/film assembly at 533 K for 1 h for nanorods of 300 nm diameter and 5 h for nanorods of 65 nm diameter, the samples were crystallized at 443 K under vacuum for 40 h to fully develop the crystallites.[31] Thin slices of the cross section of iPS nanorods/bulk film with protruding nanorods for the SEM and micro-XRD analysis were cut using a razor blade after removal of the AAO template.

Characterization. The morphologies of AAO templates and iPS nanorods were observed using an S-4300SE (Hitachi Co., Ltd.) SEM at an acceleration voltage of 5 kV. Micro-XRD measurements were carried out on the BL40XU beamline of SPring-8 in Hyogo, Japan. The wavelength of the X-ray beam was 0.082656 nm, and the beam size was 2.9 μm × 3.5 μm as half-width. The samples were moved stepwise at 5 μm intervals and X-ray irradiated for 0.6 s.

dx.doi.org/10.1021/mz400136d | *ACS Macro Lett.* 2013, 2, 414−418

■ ASSOCIATED CONTENT

Supporting Information

2D micro-XRD patterns in the radial direction of spherulite, and nucleation density of iPS film evaluated by POM observation. This material is available free of charge via the Internet at http://pubs.acs.org.

■ AUTHOR INFORMATION

Corresponding Author

*E-mail: takahara@cstf.kyushu-u.ac.jp.

Notes

The authors declare no competing financial interest.

■ ACKNOWLEDGMENTS

The synchrotron radiation experiments were performed at BL40XU in the SPring-8 facility with the approval of the Japan Synchrotron Radiation Institute (JASRI) (Proposal Nos. 2012A1291, 2012B1231)

■ REFERENCES

(1) Granasy, L.; Pusztai, T.; Borzsonyi, T.; Warren, J. A.; Douglas, J. F. *Nat. Mater.* **2004**, *3*, 645−650.
(2) Strobl, G. *The Physics of Polymers*; Springer: Berlin, 1997;
(3) Keller, A. *Nature* **1952**, *169*, 913−914.
(4) Bassett, D. C.; Vaughan, A. S. *Polymer* **1985**, *26*, 717−725.
(5) Cheng, S. Z. D.; Wunderlich, B. *J. Polym. Sci., Part B: Polym. Phys.* **1986**, *24*, 595−617.
(6) Keith, H. D.; Padden, F. J., Jr. *J. Polym. Sci., Part B: Polym. Phys.* **1987**, *25*, 2371−2392.
(7) Lotz, B.; Wittmann, J. C.; Lovinger, A. J. *Polymer* **1996**, *37*, 4979−4992.
(8) Frank, C. W.; Rao, V.; Despotopoulou, M. M.; Pease, R. F. W.; Hinsberg, W. D.; Miller, R. D.; Rabolt, J. F. *Science* **1996**, *273*, 912−915.
(9) Li, L.; Chan, C. M.; Yeung, K. L.; Li, J. X.; Ng, K. M.; Lei, Y. G. *Macromolecules* **2001**, *34*, 316−325.
(10) Massa, M. V.; Carvalho, J. L.; Dalnoki-Veress, K. *Eur. Phys. J. E* **2003**, *12*, 111−117.
(11) Hu, Z. J.; Jonas, A. M. *Soft Matter* **2010**, *6*, 21−28.
(12) Zhu, L.; Cheng, S. Z. D.; Calhoun, B. H.; Ge, Q.; Quirk, R. P.; Thomas, E. L.; Hsiao, B. S.; Yeh, F. J.; Lotz, B. *J. Am. Chem. Soc.* **2000**, *122*, 5957−5967.
(13) Loo, Y. L.; Register, R. A.; Ryan, A. J. *Phys. Rev. Lett.* **2000**, *84*, 4120−4123.
(14) Huang, P.; Guo, Y.; Quirk, R. P.; Ruan, J. J.; Lotz, B.; Thomas, E. L.; Hsiao, B. S.; Avila-Orta, C. A.; Sics, I.; Cheng, S. Z. D. *Polymer* **2006**, *47*, 5457−5466.
(15) Chung, T. M.; Wang, T. C.; Ho, R. M.; Sun, Y. S.; Ko, B. T. *Macromolecules* **2010**, *43*, 6237−6240.
(16) Nojima, S.; Ohguma, Y.; Kadena, K.; Ishizone, T.; Iwasaki, Y.; Yamaguchi, K. *Macromolecules* **2010**, *43*, 3916−3923.
(17) Steinhart, M.; Göring, P.; Dernaika, H.; Prabhukaran, M.; Gösele, U.; Hempel, E.; Thurn-Albrecht, T. *Phys. Rev. Lett.* **2006**, *97*, 027801.
(18) Wu, H.; Wang, W.; Yang, H.; Su, Z. *Macromolecules* **2007**, *40*, 4244−4249.
(19) Shin, K.; Woo, E.; Jeong, Y. G.; Kim, C.; Huh, J.; Kim, K. W. *Macromolecules* **2007**, *40*, 6617−6623.
(20) Garcia-Gutierrez, M. C.; Linares, A.; Hernandez, J. J.; Rueda, D. R.; Ezquerra, T. A.; Poza, P.; Davies, R. J. *Nano Lett.* **2010**, *10*, 1472−1476.
(21) Lutkenhaus, J. L.; McEnnis, K.; Serghei, A.; Russell, T. P. *Macromolecules* **2010**, *43*, 3844−3850.
(22) Duran, H.; Steinhart, M.; Butt, H. J.; Floudas, G. *Nano Lett.* **2011**, *11*, 1671−1675.
(23) Wu, H.; Su, Z.; Takahara, A. *Soft Matter* **2012**, *8*, 3180−3184.
(24) Park, K.; Choi, K.; Lee, J. H.; Park, S. H.; Lee, S. C.; Lee, H. S. *ACS Macro Lett.* **2012**, *1*, 110−114.
(25) Michell, R. M.; Lorenzo, A. T.; Muller, A. J.; Lin, M.-C.; Chen, H.-L.; Blaszczyk-Lezak, I.; Martin, J.; Mijangos, C. *Macromolecules* **2012**, *45*, 1517−1528.
(26) Wu, H.; Su, Z.; Takahara, A. *RSC Adv.* **2012**, *2*, 8707−8712.
(27) Maiz, J.; Martin, J.; Mijangos, C. *Langmuir* **2012**, *28*, 12296−12303.
(28) Li, M.; Wu, H.; Huang, Y.; Su, Z. *Macromolecules* **2012**, *45*, 5196−5200.
(29) Guan, Y.; Liu, G.; Gao, P.; Li, L.; Ding, G.; Wang, D. *ACS Macro Lett.* **2013**, *2*, 181−184.
(30) Natta, G.; Pino, P.; Corradini, P.; Danusso, F.; Mantica, E.; Mazzanti, G.; Moraglio, G. *J. Am. Chem. Soc.* **1955**, *77*, 1708−1710.
(31) Hammel, R.; MacKnight, W. J.; Karasz, F. E. *J. Appl. Phys.* **1975**, *46*, 4199−4203.
(32) Ebert, F.; Thurn-Albrecht, T. *Macromolecules* **2003**, *36*, 8685−8694.
(33) Amelino, L.; Martuscelli, E.; Sellitti, C.; Silvestre, C. *Polymer* **1990**, *31*, 1051−1057.
(34) Ma, Y.; Hu, W. B.; Hobbs, J.; Reiter, G. *Soft Matter* **2008**, *4*, 540−543.
(35) Masuda, H.; Fukuda, K. *Science* **1995**, *268*, 1466−1468.
(36) Li, A. P.; Muller, F.; Birner, A.; Nielsch, K.; Gösele, U. *J. Appl. Phys.* **1998**, *84*, 6023−6026.